

## Giant Bulk Photovoltaic Effect in Vinylene-Linked Hybrid Heterocyclic Polymer

Shi Liu, Fan Zheng, and Andrew M. Rappe

*J. Phys. Chem. C*, **Just Accepted Manuscript** • DOI: 10.1021/acs.jpcc.7b00374 • Publication Date (Web): 02 Mar 2017

Downloaded from <http://pubs.acs.org> on March 8, 2017

### Just Accepted

“Just Accepted” manuscripts have been peer-reviewed and accepted for publication. They are posted online prior to technical editing, formatting for publication and author proofing. The American Chemical Society provides “Just Accepted” as a free service to the research community to expedite the dissemination of scientific material as soon as possible after acceptance. “Just Accepted” manuscripts appear in full in PDF format accompanied by an HTML abstract. “Just Accepted” manuscripts have been fully peer reviewed, but should not be considered the official version of record. They are accessible to all readers and citable by the Digital Object Identifier (DOI®). “Just Accepted” is an optional service offered to authors. Therefore, the “Just Accepted” Web site may not include all articles that will be published in the journal. After a manuscript is technically edited and formatted, it will be removed from the “Just Accepted” Web site and published as an ASAP article. Note that technical editing may introduce minor changes to the manuscript text and/or graphics which could affect content, and all legal disclaimers and ethical guidelines that apply to the journal pertain. ACS cannot be held responsible for errors or consequences arising from the use of information contained in these “Just Accepted” manuscripts.

# Giant Bulk Photovoltaic Effect in Vinylene-Linked Hybrid Heterocyclic Polymer

Shi Liu,<sup>\*,†</sup> Fan Zheng,<sup>‡</sup> and Andrew M. Rappe<sup>\*,‡</sup>

<sup>†</sup>*Extreme Materials Initiative, Geophysical Laboratory, Carnegie Institution for Science,  
Washington, D.C. 20015-1305 USA*

<sup>‡</sup>*Department of Chemistry, University of Pennsylvania, Philadelphia, Pennsylvania  
19104-6323, USA*

E-mail: sliu@carnegiescience.edu; rappe@sas.upenn.edu

## Abstract

The bulk photovoltaic effect refers to the generation of a steady photocurrent from a homogeneous noncentrosymmetric material. It offers an alternative to the traditional  $p$ - $n$  junction-based photovoltaic mechanism to directly convert sunlight to electricity. In this work, we investigate the bulk photovoltaic effect in low-dimensional polar organic materials with first-principles density functional theory calculations and shift current theory. With a strategy designed to break the inversion symmetry along the polymer chain, we demonstrate that conjugated vinylene-linked hybrid heterocyclic polymers can produce strong bulk photovoltaic response to light, outperforming benchmark inorganic materials. The high current density results from the delocalized wavefunctions, composed mainly of carbon  $p$  orbitals. The great structural and electronic flexibility of polymers offers a robust paradigm to enhance the shift current response through chemical and physical modifications. The development of polymer blends with polymers of different band gaps potentially enables the utilization of the whole visible light spectrum for energy conversion.

## Introduction

The bulk photovoltaic effect (BPVE) is a phenomenon in which a steady photocurrent and above-band-gap photovoltage are generated from a single-phase noncentrosymmetric bulk material.<sup>1-5</sup> This phenomenon was first observed more than fifty years ago in ferroelectric materials<sup>1,2</sup> and modeled theoretically.<sup>6,7</sup> However, the connection between theory and experiment remained poorly understood until recent *ab initio* investigations.<sup>8</sup> The BPVE, in particular, the shift current mechanism,<sup>8</sup> is fundamentally different from the traditional *p-n* junction-based photovoltaic (PV) mechanism. The driving force that separates photoexcited carriers in a *p-n* junction solar cell is the built-in electric field at the heterointerface of two semiconductors. In the shift current bulk photovoltaic mechanism, the driving force is the coherent evolution of excited electron (hole) wavepackets. The most attractive feature of the BPVE is the generation of above-band-gap photovoltages, which offers a route<sup>9</sup> to overcome the Shockley-Queisser limit of the *p-n* junction PV technology, where the open-circuit voltage is limited by the fundamental band gap of bulk semiconductors.

Only noncentrosymmetric materials exhibit the BPVE. Ferroelectric materials, characterized by broken inversion symmetry and switchable bulk polarization, guarantee the generation of a bulk photocurrent upon light excitation. However, ferroelectrics often possess large band gaps that prevent the absorption of visible light, causing low conversion efficiency. Recently, there is renewed interest toward applying the BPVE for energy conversion, inspired by the realization of above-band-gap open-circuit voltage in ferroelectrics and the synthesis of novel ferroelectrics with band gap in visible light region.<sup>10-15</sup> In particular, BiFeO<sub>3</sub> (BFO) is found to exhibit strong photovoltaic response.<sup>16-22</sup> Although various contributions to the photocurrent in BFO were suggested, our first-principles calculations demonstrated that the shift current is the main mechanism for the BPVE in single-domain BFO, and the theoretical photoresponse agrees with the measured current magnitudes.<sup>23</sup> In addition to BFO, many low band-gap ferroelectrics are also designed and synthesized, with the shift current method applied to evaluate their BPVE performance.<sup>11,24-33</sup> The band gap of BFO

1  
2  
3 (2.7 eV),<sup>34</sup> though smaller than typical ferroelectrics, is still relatively high compared to  
4 silicon, wasting a large part of the visible light. Therefore, discovering and designing new  
5 low band-gap materials (polar but not necessarily ferroelectric) with high BPVE is always  
6 imperative for the development of solar cells of high power conversion efficiency.  
7  
8

9  
10  
11 Conjugated organic polymers have been used in many electro-optical devices, such as  
12 organic light-emitting diodes,<sup>35,36</sup> photodetectors,<sup>37</sup> and field effect transistors.<sup>38-40</sup> The con-  
13 jugated organic polymers are also promising candidates for next-generation light absorbers  
14 in solar cells,<sup>41,42</sup> due to their exceptional properties such as high internal quantum efficiency  
15 (photon to electron efficiency),<sup>43</sup> light weight, flexibility and the low cost to synthesize. Fur-  
16 thermore, the structural flexibility and tunability of polymers provide a rich playground for  
17 the design of functional polymers with desired electronic properties. For example, the band  
18 gap of conjugated polymers can be easily tuned by incorporating different donor-acceptor  
19 units or by introducing aromatic and quinoid units in an alternating sequence.<sup>44-48</sup> How-  
20 ever, there is very limited study of the BPVE response in polymeric materials.<sup>12</sup> The BPVE  
21 of polyvinylidene fluoride (PVDF), a prototypical organic ferroelectric, was measured more  
22 than thirty years ago,<sup>49</sup> but its large band gap and small photocurrent prevent its applica-  
23 tion to solar energy conversion. Therefore, the design of polymers with small band gaps and  
24 strong BPVE is a compelling goal. While the shift current has been calculated on many  
25 non-oxide semiconductors,<sup>50-52</sup> there is little theoretical investigation on low-dimensional  
26 materials,<sup>53</sup> although reduced size and dimensionality are predicted to enhance the photore-  
27 sponse.<sup>9,18</sup> In this work, we compute the shift current responses for various one-dimensional  
28 vinylene-linked heterocyclic polymers and find that these polar polymers can generate giant  
29 bulk photocurrents along the polymer chain, outperforming benchmark bulk photovoltaic  
30 materials such as BFO.  
31  
32  
33  
34  
35  
36  
37  
38  
39  
40  
41  
42  
43  
44  
45  
46  
47  
48  
49  
50  
51  
52  
53  
54  
55  
56  
57  
58  
59  
60

## Methods

Shift current is a second-order nonlinear optical effect with coherent excited states (wave packets) as the carriers, resulting from two successive interactions between the photons and the electrons (or holes).<sup>54</sup> Using perturbation theory, the shift current response ( $\sigma$ ) can be computed from first-principles:

$$\begin{aligned}
 J_q &= \sigma_{rsq} E_r E_s \\
 \sigma_{rsq}(\omega) &= e \sum_{n', n''} \int d\mathbf{k} \mathcal{I}(n', n'', \mathbf{k}, \omega) \mathcal{R}(n', n'', \mathbf{k}) \\
 \mathcal{I}(n', n'', \mathbf{k}, \omega) &= \left( \frac{e}{m\hbar\omega} \right)^2 (f[n''\mathbf{k}] - f[n'\mathbf{k}]) \\
 &\quad \times \langle n'\mathbf{k} | \hat{P}_r | n''\mathbf{k} \rangle \langle n''\mathbf{k} | \hat{P}_s | n'\mathbf{k} \rangle \\
 &\quad \times \delta(\omega_{n''}(\mathbf{k}) - \omega_{n'}(\mathbf{k}) \pm \omega) \\
 \mathcal{R}(n', n'', \mathbf{k}) &= \left( -\frac{\partial \phi_{n'n''}(\mathbf{k}, \mathbf{k})}{\partial k_q} - [\chi_{n''q}(\mathbf{k}) - \chi_{n'q}(\mathbf{k})] \right)
 \end{aligned}$$

where shift current response ( $\sigma_{rsq}$ ) is the product of the transition intensity ( $\mathcal{I}$ ) and shift vector ( $\mathcal{R}$ ), representing the probability of excitations and the associated distance for the excited shift current carriers.  $E_r$  is the  $r$ th component of the electric field of the light,  $\omega$  is the light frequency,  $f$  is the Fermi filling,  $n$  and  $\mathbf{k}$  are the band index and wavevector of the wavefunction, respectively;  $\phi_{n',n''}$  is the phase of the momentum matrix element for transition from band  $n'$  to  $n''$ , and  $\chi_n$  is the Berry connection for state at band  $n$  and  $\mathbf{k}$  point.

The plane-wave density functional theory (DFT) code QUANTUM-ESPRESSO is used to optimize the structure and compute the electronic properties of polymers with periodic boundary conditions (PBCs). The generalized gradient approximation (GGA) functional<sup>55</sup> is used with norm-conserving, designed nonlocal pseudopotentials generated with the OPIUM package.<sup>56,57</sup> In our calculations, a plane-wave cutoff of 50 Ry is sufficient to converge the

total energy. In order to study the single polymer chain, a large box with vacuum more than 10 Å along  $y$  and  $z$  directions is used to avoid interactions between different images due to PBCs. All the structures are relaxed with a force threshold less than 0.025 eV/Å and an  $8 \times 2 \times 2$   $k$ -point grid. With the relaxed structure and the converged charge density, a non-self-consistent calculation on a much denser  $k$ -point grid is performed to converge the shift current response. Due to the known deficiency of the GGA functional for band gap predictions, the HSE<sup>58</sup> and B3LYP<sup>59</sup> functionals incorporating exact exchange included are used to correct the underestimated band gaps.

## Results and Discussion

### Structural Properties

The breaking of inversion symmetry is necessary for the shift current response. However, non-polar materials (*e.g.*, hexagonal boron nitride) with broken inversion symmetry will only possess shift current under polarized light. Generating shift currents from unpolarized light requires the material to be both noncentrosymmetric and polar. To break the inversion symmetry along the polymer chain, we design vinylene-linked hybrid heterocyclic polymers by incorporating two five-membered rings, each containing a different functional group ( $A/B$ ). However, this is not sufficient, as the polymer dipole is perpendicular to the chain axis (Fig. 1b). We further introduce alternating  $A-B$  and  $B-A$  distances by increasing the number of vinylene groups connecting  $B$  to  $A$  (r1, Fig.1c). We explore polymers containing two of the four functional groups, BH, CH<sub>2</sub>, NH, and O. It is noted that the BH heterocyclic ring is quinoidal as it has two electrons fewer than the other aromatic heterocyclic rings. The optimized structures are shown in Figure 2. The bond length alternation (BLA), defined as the difference between the length of the nominally single and double bonds along the polymer chain, reflects the  $\pi$ -conjugated behavior. We calculate the BLA for each polymer by taking the difference between the bond length of the C-C bond attached to the heterocyclic ring

1  
2  
3 and the C-C bond in the adjacent vinylene linker group.<sup>48</sup> Within this definition, a positive  
4  
5  
6  
7  
8  
9  
10  
11  
12  
13  
14  
15  
16  
17  
18  
19  
20  
21  
22  
23  
24  
25  
26  
27  
28  
29  
30  
31  
32  
33  
34  
35  
36  
37  
38  
39  
40  
41  
42  
43  
44  
45  
46  
47  
48  
49  
50  
51  
52  
53  
54  
55  
56  
57  
58  
59  
60  
and the C-C bond in the adjacent vinylene linker group.<sup>48</sup> Within this definition, a positive  
BLA value suggests aromatic behavior while a negative BLA value indicates quinoidal char-  
acter (Fig. 2). We find that the BH heterocyclic ring gives rise to strong quinoidal character  
regardless of the type of the other functional group.

## Electronic Structure

We investigate the electronic structure of the designed hybrid heterocyclic polymers by cal-  
culating the band structures along the  $\Gamma - X$  path in the irreducible Brillouin zone (Fig. 3).  
We find that polymers containing boron (*e.g.*, NH-BH,  $E_g = 0.68$  eV) have larger band gaps  
at the X point compared to their counterparts without boron (*e.g.*, NH-O,  $E_g = 0.58$  eV).  
The larger band gap for polymers with the BH functional group is mainly caused by the  
reduced band width of the lowest conduction band (CB). For a conjugated polymer, the  
width of a band reflects the orbital interactions along the polymer chain: a wide dispersive  
band indicates orbital delocalization and a narrow flat band denotes orbital localization. The  
small band width of the lowest CB for CH<sub>2</sub>-NH, NH-BH, and O-BH polymers is attributed  
to the highly quinoidal character of the BH cyclic ring, consistent with the BLA analysis.

To provide insights into the electronic structure, we compare the atom-resolved den-  
sity of states of NH-BH and O-NH polymers. Though orbitals from carbon atoms at the  
backbone/cyclic rings dominate the states near the Fermi energy, the boron has substantial  
contributions to band edge states as well, while orbitals from O/N atoms have little contri-  
bution. The presence of boron interrupts the *p*-orbital hybridization of carbon atoms along  
the polymer chain, thus reducing the electron delocalization and the CB width, increasing  
the band gap.

We further study the bonding character by examining the CB wavefunctions. As shown  
in Fig. 5, due to the presence of boron, the wavefunctions and the bonding characters are  
very similar at the  $\Gamma$  and X points, except some small difference within the BH-cyclic ring  
(outlined by the rectangular boxes), which leads to a modest energy change along the  $\Gamma - X$

1  
2  
3 path and thus small band dispersion. By replacing BH with O and NH with CH<sub>2</sub>, the  
4 bonding character at the  $\Gamma$  point shows a mix of aromatic and quinoidal characters along  
5 the chain, but it becomes purely quinoidal at the X point. Moreover, as illustrated from the  
6 real-space wavefunctions, the  $\Gamma$  point wavefunction shows non-bonding carbon atoms, which  
7 further increases its energy. The large difference in bonding characters at the  $\Gamma$  and X points  
8 causes a large energy difference and the wide band width.  
9

10  
11 Because semilocal density functional such as GGA are known to underestimate the band  
12 gap, we perform calculations with hybrid density functionals to validate the calculated GGA  
13 band structures. Shown in Fig. 6 are the band structures obtained with GGA and HSE  
14 for NH-BH and CH<sub>2</sub>-O polymers. Though the GGA functional underestimates the band  
15 gap value almost by half compared to HSE, the band dispersions from these two density  
16 functionals are similar. Previous studies showed that the B3LYP functional predicts band  
17 gap values closer to experimental results for conjugated polymers.<sup>48</sup> We also evaluate the  
18 band gaps with B3LYP functional. We find that the B3LYP further increases the band gap  
19 by 0.25 eV compared to HSE results: NH-BH, GGA 0.68 eV, HSE 1.05 eV, B3LYP 1.37 eV;  
20 CH<sub>2</sub>-O, GGA 0.22 eV, HSE 0.52 eV, B3LYP 0.77 eV. It is noted that the band dispersion  
21 from B3LYP is also similar to those obtained with GGA and HSE: in these cases, the exact  
22 exchange tends to rigidly shift the GGA bands without changing the orbital characters  
23 significantly. For this reason, we decide to compute the shift current response based on the  
24 GGA functional due to its low computational cost.  
25  
26  
27  
28  
29  
30  
31  
32  
33  
34  
35  
36  
37  
38  
39  
40  
41  
42  
43  
44  
45

## 46 Shift Current Response

47  
48 We calculate the shift current response along the polymer chain in response to both parallel  
49 ( $xxX$ ) and perpendicular ( $yyX$ ) linearly polarized light (Fig. 7). The studied conjugated  
50 polymers all show strong BPVE, with the maximum current response (NH-BH polymer)  
51 surpassing the maximum BPVE for inorganic ferroelectric BiFeO<sub>3</sub> and solar materials such  
52 as MAPbI<sub>3</sub>. Previous studies suggested that materials characterized by strongly asymmetric  
53  
54  
55  
56  
57  
58  
59  
60

1  
2  
3 and delocalized valence and/or conduction states tend to have larger shift vectors. Typi-  
4 cal ferroelectrics such as  $\text{PbTiO}_3$ , although they have large polarization, are not ideal for  
5 generating shift currents because the band edge states usually consist of non-bonding, lo-  
6 calized states. On the contrary, the delocalized  $p$  orbitals along the backbone of conjugated  
7 polymers are beneficial for supporting current-carrying excited wavepacket states. The shift  
8 current responses of polymers also appear to be highly tunable, as different combinations  
9 of functional groups give rise to currents peaking at different light frequencies. A designed  
10 polymer blend with different types of hybrid heterocyclic polymers may use the whole visible  
11 light spectrum, maximizing the output current from sun light.  
12  
13  
14  
15  
16  
17  
18  
19  
20  
21  
22  
23

## 24 **Designed Optimization**

25  
26 The BVPE in vinylene-linked hybrid heterocyclic polymers can be further enhanced with  
27 various physical and chemical strategies (Fig. 8). Here we demonstrate several possible  
28 approaches. First, increase the electronegativity difference between A and B functional  
29 groups will increase the magnitude of symmetry breaking. We find that replacing the  
30 hydrogen atom attached to the boron with  $-\text{CF}_3$  group results in a larger shift current in  
31 NH-BCF<sub>3</sub> polymer. The second approach is to increase the difference between  $r_1$  and  $r_2$   
32 by introducing more vinylene linking units between A and B (shown as NH-BH; $r_1=(\text{CH})_8$ ).  
33 We also find that replacing some backbone hydrogen atoms with highly electronegative  
34 fluorine atoms (NH-BH;F and NH-BH; $r_1=(\text{CH})_8$  polymers) is beneficial. Lastly, increasing  
35 the polymer density per unit volume enhances the response magnitude. Through these  
36 optimizations, the conjugated polymer can even surpass the peak shift current of the best  
37 known inorganic bulk photovoltaic material,  $\text{LiAsSe}_2$ .<sup>50</sup> Because the electron-hole screening  
38 is generally weaker in low-dimensional materials,<sup>60,61</sup> additional design principles, such as  
39 the usage of substrate of high dielectric constant, can be used to help the suppression of  
40 excitonic effect along the polymer chain. It is noted that we assume the polymer chains will  
41 pack in parallel direction to maximize the current response in our calculations. Ferroelectric  
42  
43  
44  
45  
46  
47  
48  
49  
50  
51  
52  
53  
54  
55  
56  
57  
58  
59  
60

1  
2  
3 polymers such as PVDF can form polar domains with polymer chains stacked in parallel  
4  
5 directions.  
6  
7

## 8 9 10 **Conclusion**

11  
12 We computationally designed a series of polar, conjugated polymers by incorporating two  
13 different heterocyclic rings and varying the number of vinylene linkage groups. Our first-  
14 principles calculations reveal that the presence of boron gives rise to strong quinoidal charac-  
15 ter, which has a strong influence on the conduction band dispersion and band gap values. All  
16 studied polymers possess very high BPVE response, surpassing benchmark materials such  
17 as BiFeO<sub>3</sub> and MAPbI<sub>3</sub>, due to the diffuse, delocalized *p* states at the band edge. The band  
18 gaps of the conjugated polymers can easily be tuned by choosing different functional groups  
19 in the heterocyclic rings. We propose several chemical and physical approaches to further  
20 enhance the shift current response. One of the expected experimental challenges would be  
21 aligning the polar polymer chains to minimize the current cancellation. Further studies,  
22 both theory and experiments, are required to reveal the synthetic conditions/approaches to  
23 exploit the high BPVE of polymers demonstrated in this work.  
24  
25  
26  
27  
28  
29  
30  
31  
32  
33  
34  
35  
36  
37  
38  
39

## 40 **Acknowledgement**

41  
42  
43 SL and FZ contributed equally to this work. SL is supported by the Carnegie Institution  
44 for Science. This work was supported by the Department of Energy under grant DE-FG02-  
45 07ER46431. Computational support was provided by the National Energy Research Scientific  
46 Computing Center (NERSC).  
47  
48  
49  
50  
51  
52  
53  
54  
55  
56  
57  
58  
59  
60

## References

- (1) Chynoweth, A. G. Surface Space-charge Layers in Barium Titanate. *Phys. Rev.* **1956**, *102*, 705–14.
- (2) Chen, F. S. Optically Induced Change of Refractive Indices in LiNbO<sub>3</sub> and LiTaO<sub>3</sub>. *J. Appl. Phys.* **1969**, *40*, 3389–96.
- (3) Glass, A. M.; von der Linde, D.; Negran, T. J. High-voltage Bulk Photovoltaic Effect and Photorefractive Process in LiNbO<sub>3</sub>. *Appl. Phys. Lett.* **1974**, *25*, 233–5.
- (4) Fridkin, V.; Grekov, A.; Ionov, P.; Rodin, A.; Savchenko, E.; Mikhailina, K. Photoconductivity in Certain Ferroelectrics. *Ferroelectrics* **1974**, *8*, 433–435.
- (5) Fridkin, V. M. Bulk Photovoltaic Effect in Noncentrosymmetric Crystals. *Crystallog. Rep.* **2001**, *46*, 654–8.
- (6) Belinicher, V. I.; Kanaev, I. F.; Malinovsky, V. K.; Sturman, B. Theory of Photogalvanic Effect in Ferroelectrics. *Ferroelectrics* **1978**, *22*, 647–8.
- (7) Sturman, B.; Carrascosa, M.; Agullo-Lopez, F. Light-induced Charge Transport in LiNbO<sub>3</sub> Crystals. *Phys. Rev. B* **2008**, *78*, 245114–1–8.
- (8) Young, S. M.; Rappe, A. M. First Principles Calculation of the Shift Current Photovoltaic Effect in Ferroelectrics. *Phys. Rev. Lett.* **2012**, *109*, 116601.
- (9) Spanier, J. E.; Fridkin, V. M.; Rappe, A. M.; Akbashev, A. R.; Polemi, A.; Qi, Y.; Gu, Z.; Young, S. M.; Hawley, C. J.; Imbrenda, D.; Xiao, G.; Bennett-Jackson, A. L.; Johnson, C. L. Power Conversion Efficiency Exceeding the Shockley–Queisser Limit in a Ferroelectric Insulator. *Nat. Photonics* **2016**, *10*, 611–616.
- (10) Bennett, J. W.; Grinberg, I.; Rappe, A. M. New Highly Polar Semiconductor Ferroelectrics through d<sup>8</sup> Cation-O Vacancy Substitution into PbTiO<sub>3</sub>: A Theoretical Study. *J. Am. Chem. Soc.* **2008**, *130*, 17409–12.

- 1  
2  
3  
4 (11) Grinberg, I.; West, D. V.; Torres, M.; Gou, G.; Stein, D. M.; Wu, L.; Chen, G.;  
5 Gallo, E. M.; Akbashev, A. R.; Davies, P. K.; Spanier, J. E.; Rappe, A. M. Per-  
6 ovskites Oxides for Visible-light-adsorbing Ferroelectric and Photovoltaic Materials.  
7 *Nature* **2013**, *503*, 509–512.  
8  
9  
10  
11  
12 (12) K.Vijayaraghavan, R.; J.Meskers, S. C.; Rahim, M. A.; Das, S. Bulk Photovoltaic Effect  
13 in an Organic Polar Crystal. *Chem. Commun.* **2014**, *50*, 6530–6533.  
14  
15  
16  
17 (13) Somma, C.; Reimann, K.; Flytzanis, C.; Elsaesser, T.; Woerner, M. High-Field Tera-  
18 hertz Bulk Photovoltaic Effect in Lithium Niobate. *Phys. Rev. Lett.* **2014**, *112*, 146602.  
19  
20  
21  
22 (14) Zenkevich, A.; Matveyev, Y.; Maksimova, K.; Gaynutdinov, R.; Tolstikhina, A.; Frid-  
23 kin, V. Giant Bulk Photovoltaic Effect in Thin Ferroelectric BaTiO<sub>3</sub> Films. *Phys. Rev.*  
24 *B* **2014**, *90*, 161409.  
25  
26  
27  
28  
29 (15) Pérez-Tomás, A.; Lira-Cantú, M.; Catalan, G. Above-Bandgap Photovoltages in Anti-  
30 ferroelectrics. *Adv. Mater.* **2016**,  
31  
32  
33  
34 (16) Choi, T.; Lee, S.; Choi, Y.; Kiryukhin, V.; Cheong, S.-W. Switchable Ferroelectric  
35 Diode and Photovoltaic Effect in BiFeO<sub>3</sub>. *Science* **2009**, *324*, 63–6.  
36  
37  
38  
39 (17) Yang, S.; Seidel, J.; Byrnes, S. J.; Schafer, P.; Yang, C.-H.; Rossel, M.; Yu, P.; Chu, Y.-  
40 H.; Scott, J. F.; Ager, J. W.; Martin, L.; Ramesh, R. Above-bandgap Voltages from  
41 Ferroelectric Photovoltaic Devices. *Nat. Nano.* **2010**, *5*, 143–7.  
42  
43  
44  
45  
46 (18) Alexe, M.; Hesse, D. Tip-enhanced photovoltaic effects in bismuth ferrite. *Nat. Comms.*  
47 **2011**, *2*, 256.  
48  
49  
50  
51 (19) Bhatnagar, A.; Roy Chaudhuri, A.; Heon Kim, Y.; Hesse, D.; Alexe, M. Role of Domain  
52 Walls in the Abnormal Photovoltaic Effect in BiFeO<sub>3</sub>. *Nat. Commun.* **2013**, *4*.  
53  
54  
55  
56 (20) Seidel, J.; Fu, D. Y.; Yang, S. Y.; Alarcon-Llado, E.; Wu, J. Q.; Ramesh, R.; Ager, J. W.  
57  
58  
59  
60

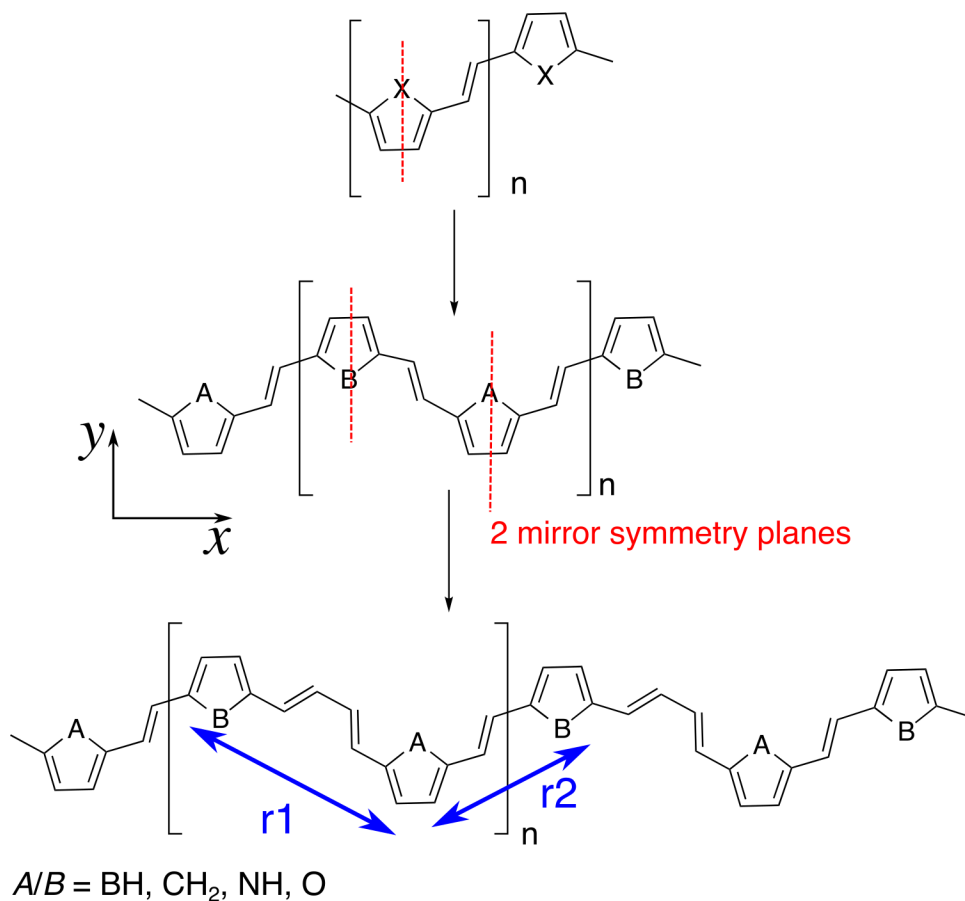
- 1  
2  
3 Efficient Photovoltaic Current Generation at Ferroelectric Domain Walls. *Phys. Rev. Lett.* **2011**, *107*, 126805.  
4  
5  
6  
7  
8  
9 (21) Ji, W.; Yao, K.; Liang, Y. C. Evidence of Bulk Photovoltaic Effect and Large Tensor  
10 Coefficient in Ferroelectric BiFeO<sub>3</sub> Thin Films. *Phys. Rev. B* **2011**, *84*, 094115.  
11  
12  
13 (22) Yang, S. Y. et al. Photovoltaic Effects in BiFeO<sub>3</sub>. *Appl. Phys. Lett.* **2009**, *95*, 062909–  
14 1–3.  
15  
16  
17  
18 (23) Young, S. M.; Zheng, F.; Rappe, A. M. First-Principles Calculation of the Bulk Pho-  
19 tovoltaic Effect in Bismuth Ferrite. *Phys. Rev. Lett.* **2012**, *109*, 236601.  
20  
21  
22  
23 (24) Nechache, R.; Harnagea, C.; Licoccia, S.; Traversa, E.; Ruediger, A.; Pignolet, A.;  
24 Rosei, F. Photovoltaic Properties of Bi<sub>2</sub>FeCrO<sub>6</sub> Epitaxial Thin Films. *Appl. Phys. Lett.*  
25 **2011**, *98*, 202902.  
26  
27  
28  
29  
30 (25) Nechache, R.; Harnagea, C.; Li, S.; Cardenas, L.; Huang, W.; Chakrabartty, J.; Ro-  
31 sei, F. Bandgap Tuning of Multiferroic Oxide Solar Cells. *Nat. Photonics* **2014**, *9*,  
32 61–67.  
33  
34  
35  
36  
37 (26) Sipe, J. E.; Shkrebtii, A. I. Second-order Optical Response in Semiconductors. *Phys.*  
38 *Rev. B* **2000**, *61*, 5337–52.  
39  
40  
41  
42 (27) von Baltz, R.; Kraut, W. Theory of the bulk photovoltaic effect in pure crystals. *Phys.*  
43 *Rev. B* **1981**, *23*, 5590–6.  
44  
45  
46  
47 (28) Wang, F.; Young, S. M.; Zheng, F.; Grinberg, I.; Rappe, A. M. Substantial Bulk  
48 Photovoltaic Effect Enhancement Via Nanolayering. *Nat. Commun.* **2016**, *7*, 10419.  
49  
50  
51  
52 (29) Wang, F.; Rappe, A. M. First-principles Calculation of the Bulk Photovoltaic Effect in  
53 KNbO<sub>3</sub> and (K, Ba)(Ni, Nb)O<sub>3-δ</sub>. *Phys. Rev. B* **2015**, *91*.  
54  
55  
56  
57  
58  
59  
60

- 1  
2  
3  
4 (30) Young, S. M.; Zheng, F.; Rappe, A. M. First-principles Materials Design of High-  
5 performing Bulk Photovoltaics with the LiNbO<sub>3</sub> Structure. *Phys. Rev. Applied* **2015**,  
6 *4*, 054004.  
7  
8  
9  
10 (31) Wang, F.; Grinberg, I.; Rappe, A. M. Semiconducting Ferroelectric Photovoltaics  
11 through Zn<sup>2+</sup> Doping into KNbO<sub>3</sub> and Polarization Rotation. *Phys. Rev. B* **2014**,  
12 *89*, 235105.  
13  
14  
15  
16  
17 (32) Wang, F.; Grinberg, I.; Rappe, A. M. Band Gap Engineering Strategy Via Polarization  
18 Rotation in Perovskite Ferroelectrics. *Appl. Phys. Lett.* **2014**, *104*, 152903.  
19  
20  
21  
22 (33) Jiang, L.; Grinberg, I.; Wang, F.; Young, S. M.; Davies, P. K.; Rappe, A. M. Semi-  
23 conducting Ferroelectric Perovskites with Intermediate Bands Via B-site Bi<sup>+5</sup> Doping.  
24 *Phys. Rev. B* **2014**, *90*.  
25  
26  
27  
28  
29 (34) Catalan, G.; Scott, J. F. Physics and Applications of Bismuth Ferrite. *Adv. Mater.*  
30 **2009**, *21*, 2463–2485.  
31  
32  
33  
34 (35) Burroughes, J. H.; Bradley, D. D. C.; Brown, A. R.; Marks, R. N.; Mackay, K.;  
35 Friend, R. H.; Burns, P. L.; Holmes, A. B. Light-emitting Diodes Based on Conju-  
36 gated Polymers. *Nature* **1990**, *347*, 539–541.  
37  
38  
39  
40  
41 (36) Friend, R. H.; Gymer, R. W.; Holmes, A. B.; Burroughes, J. H.; Marks, R. N.; Tal-  
42 iani, C.; Bradley, D. D. C.; Santos, D. A. D.; Brdas, J. L.; Lgdlund, M.; Salaneck, W. R.  
43 Electroluminescence in Conjugated Polymers. *Nature* **1999**, *397*, 121–128.  
44  
45  
46  
47  
48 (37) Chen, S.; Teng, C.; Zhang, M.; Li, Y.; Xie, D.; Shi, G. A Flexible UV-Vis-NIR Pho-  
49 todetector based on a Perovskite/Conjugated-Polymer Composite. *Adv. Mater.* **2016**,  
50 *28*, 5969–5974.  
51  
52  
53  
54  
55 (38) Siringhaus, H.; Kawase, T.; Friend, R. H.; Shimoda, T.; Inbasekaran, M.; Wu, W.;

- 1  
2  
3  
4  
5  
6  
7  
8  
9  
10  
11  
12  
13  
14  
15  
16  
17  
18  
19  
20  
21  
22  
23  
24  
25  
26  
27  
28  
29  
30  
31  
32  
33  
34  
35  
36  
37  
38  
39  
40  
41  
42  
43  
44  
45  
46  
47  
48  
49  
50  
51  
52  
53  
54  
55  
56  
57  
58  
59  
60
- Woo, E. P. High-Resolution Inkjet Printing of All-Polymer Transistor Circuits. *Science* **2000**, *290*, 2123–2126.
- (39) Tseng, H.-R.; Phan, H.; Luo, C.; Wang, M.; Perez, L. A.; Patel, S. N.; Ying, L.; Kramer, E. J.; Nguyen, T.-Q.; Bazan, G. C.; Heeger, A. J. High-Mobility Field-Effect Transistors Fabricated with Macroscopic Aligned Semiconducting Polymers. *Adv. Mater.* **2014**, *26*, 2993–2998.
- (40) Lei, T.; Dou, J.-H.; Ma, Z.-J.; Yao, C.-H.; Liu, C.-J.; Wang, J.-Y.; Pei, J. Ambipolar Polymer Field-Effect Transistors Based on Fluorinated Isoindigo: High Performance and Improved Ambient Stability. *J. Am. Chem. Soc.* **2012**, *134*, 20025–20028.
- (41) Dou, L.; Liu, Y.; Hong, Z.; Li, G.; Yang, Y. Low-Bandgap Near-IR Conjugated Polymers/Molecules for Organic Electronics. *Chem. Rev.* **2015**, *115*, 12633–12665.
- (42) SambathKumar, B.; Kumar, P. S. V.; Deepakrao, F. S.; Iyer, S. S. K.; Subramanian, V.; Datt, R.; Gupta, V.; Chand, S.; Somanathan, N. Two Donor–One Acceptor Random Terpolymer Comprised of Diketopyrrolopyrrole Quaterthiophene with Various Donor *pi*-Linkers for Organic Photovoltaic Application. *The Journal of Physical Chemistry C* **2016**, *120*, 26609–26619.
- (43) Park, S. H.; Roy, A.; Beaupr, S.; Cho, S.; Coates, N.; Moon, J. S.; Moses, D.; Leclerc, M.; Lee, K.; Heeger, A. J. Bulk Heterojunction Solar Cells with Internal Quantum Efficiency Approaching 100%. *Nat. Photonics* **2009**, *3*, 297–302.
- (44) van Mullekom, H. Developments in the Chemistry and Band Gap Engineering of Donor–acceptor Substituted Conjugated Polymers. *Materials Science and Engineering: R: Reports* **2001**, *32*, 1–40.
- (45) Zhou, Z.-H.; Maruyama, T.; Kanbara, T.; Ikeda, T.; Ichimura, K.; Yamamoto, T.; Tokuda, K. Unique Optical and Electrochemical Properties of  $\pi$ -conjugated Electri-

- 1  
2  
3 cally Conducting Copolymers Consisting of Electron-withdrawing Pyridine Units and  
4 Electron-donating Thiophene Units. *J. Chem. Soc., Chem. Commun.* **1991**, 1210–1212.  
5  
6  
7  
8  
9 (46) Cheng, Y.-J.; Yang, S.-H.; Hsu, C.-S. Synthesis of Conjugated Polymers for Organic  
10 Solar Cell Applications. *Chem. Rev.* **2009**, *109*, 5868–5923.  
11  
12  
13 (47) Dahlstrand, C.; Jahn, B. O.; Grigoriev, A.; Villaume, S.; Ahuja, R.; Ottosson, H.  
14 Polyfulvenes: Polymers with “Handles” That Enable Extensive Electronic Structure  
15 Tuning. *J. Phys. Chem. C* **2015**, *119*, 25726–25737.  
16  
17  
18  
19  
20 (48) Wong, B. M.; Cordaro, J. G. Electronic Properties of Vinylene-Linked Heterocyclic  
21 Conducting Polymers: Predictive Design and Rational Guidance from DFT Calcula-  
22 tions. *J. Phys. Chem. C* **2011**, *115*, 18333–18341.  
23  
24  
25  
26  
27 (49) Ogden, T. R.; Gookin, D. M. Bulk Photovoltaic Effect in Polyvinylidene Fluoride. *Appl.*  
28 *Phys. Lett.* **1984**, *45*, 995.  
29  
30  
31  
32 (50) Brehm, J. A.; Young, S. M.; Zheng, F.; Rappe, A. M. First-principles Calculation of  
33 the Bulk Photovoltaic Effect in the Polar Compounds LiAsS<sub>2</sub>, LiAsSe<sub>2</sub>, and NaAsSe<sub>2</sub>.  
34 *J. Chem. Phys.* **2014**, *141*, 204704.  
35  
36  
37  
38  
39 (51) Zheng, F.; Takenaka, H.; Wang, F.; Koocher, N. Z.; Rappe, A. M. First-Principles  
40 Calculation of Bulk Photovoltaic Effect in CH<sub>3</sub>NH<sub>3</sub>PbI<sub>3</sub> and CH<sub>3</sub>NH<sub>3</sub>PbI<sub>3-x</sub>Cl<sub>x</sub>. *J.*  
41 *Phys. Chem. Lett.* **2015**, *6*, 31–37.  
42  
43  
44  
45  
46 (52) Tan, L. Z.; Rappe, A. M. Enhancement of the Bulk Photovoltaic Effect in Topological  
47 Insulators. *Phys. Rev. Lett.* **2016**, *116*, 237402.  
48  
49  
50  
51 (53) Rangel, T.; Fregoso, B. M.; Mendoza, B. S.; Morimoto, T.; Moore, J. E.;  
52 Neaton, J. B. Giant Bulk Photovoltaic Effect and Spontaneous Polarization of Single-  
53 layer Monochalcogenides. *arXiv preprint arXiv:1610.06589* **2016**,  
54  
55  
56  
57  
58  
59  
60

- 1  
2  
3  
4 (54) Tan, L. Z.; Zheng, F.; Young, S. M.; Wang, F.; Liu, S.; Rappe, A. M. Shift Current Bulk  
5 Photovoltaic Effect in Polar Materials—hybrid and Oxide Perovskites and Beyond. *npj*  
6 *Comput. Mater.* **2016**, *2*, 16026.  
7  
8  
9  
10 (55) Perdew, J. P.; Burke, K.; Ernzerhof, M. Generalized Gradient Approximation Made  
11 Simple. *Phys. Rev. Lett.* **1996**, *77*, 3865–8.  
12  
13  
14 (56) Rappe, A. M.; Rabe, K. M.; Kaxiras, E.; Joannopoulos, J. D. Optimized Pseudopotentials.  
15 *Phys. Rev. B Rapid Comm.* **1990**, *41*, 1227–30.  
16  
17  
18 (57) Ramer, N. J.; Rappe, A. M. Designed Nonlocal Pseudopotentials for Enhanced Transferability.  
19 *Phys. Rev. B* **1999**, *59*, 12471–8.  
20  
21  
22 (58) Heyd, J.; Scuseria, G. E.; Ernzerhof, M. Erratum: “Hybrid functionals based on a  
23 screened Coulomb potential” [ *J. Chem. Phys.* 118, 8207 (2003) ]. *J. Chem. Phys.*  
24 **2006**, *124*, 219906–219906.  
25  
26  
27 (59) Becke, A. Density-functional Thermochemistry. III. the Role of Exact Exchange. *J.*  
28 *Chem. Phys.* **1993**, *98*, 5648–52.  
29  
30  
31 (60) Spataru, C. D.; Ismail-Beigi, S.; Benedict, L. X.; Louie, S. G. Excitonic Effects and  
32 Optical Spectra of Single-Walled Carbon Nanotubes. *Phys. Rev. Lett.* **2004**, *92*, 077402.  
33  
34  
35 (61) Morimoto, T.; Nagaosa, N. Topological aspects of nonlinear excitonic processes in non-  
36 centrosymmetric crystals. *Phys. Rev. B* **2016**, *94*, 035117.  
37  
38  
39  
40  
41  
42  
43  
44  
45  
46  
47  
48  
49  
50  
51  
52  
53  
54  
55  
56  
57  
58  
59  
60



33  
34  
35  
36  
37  
38  
39  
40  
41  
42  
43  
44  
45  
46  
47  
48  
49  
50  
51  
52  
53  
54  
55  
56  
57  
58  
59  
60

Figure 1: Design of polar hybrid heterocyclic polymers. Starting with a typical heterocyclic polymer with only one type of five-membered ring, the inversion symmetry with respect to the bond center is broken by incorporating two five-membered rings, each bearing a different functional group ( $A/B = \text{BH}, \text{CH}_2, \text{NH}, \text{and O}$ ). Further breaking of rotation and mirror symmetry is accomplished by varying the number of vinylene linkage groups connecting  $B$  to  $A$  ( $r_1 \neq r_2$ ).

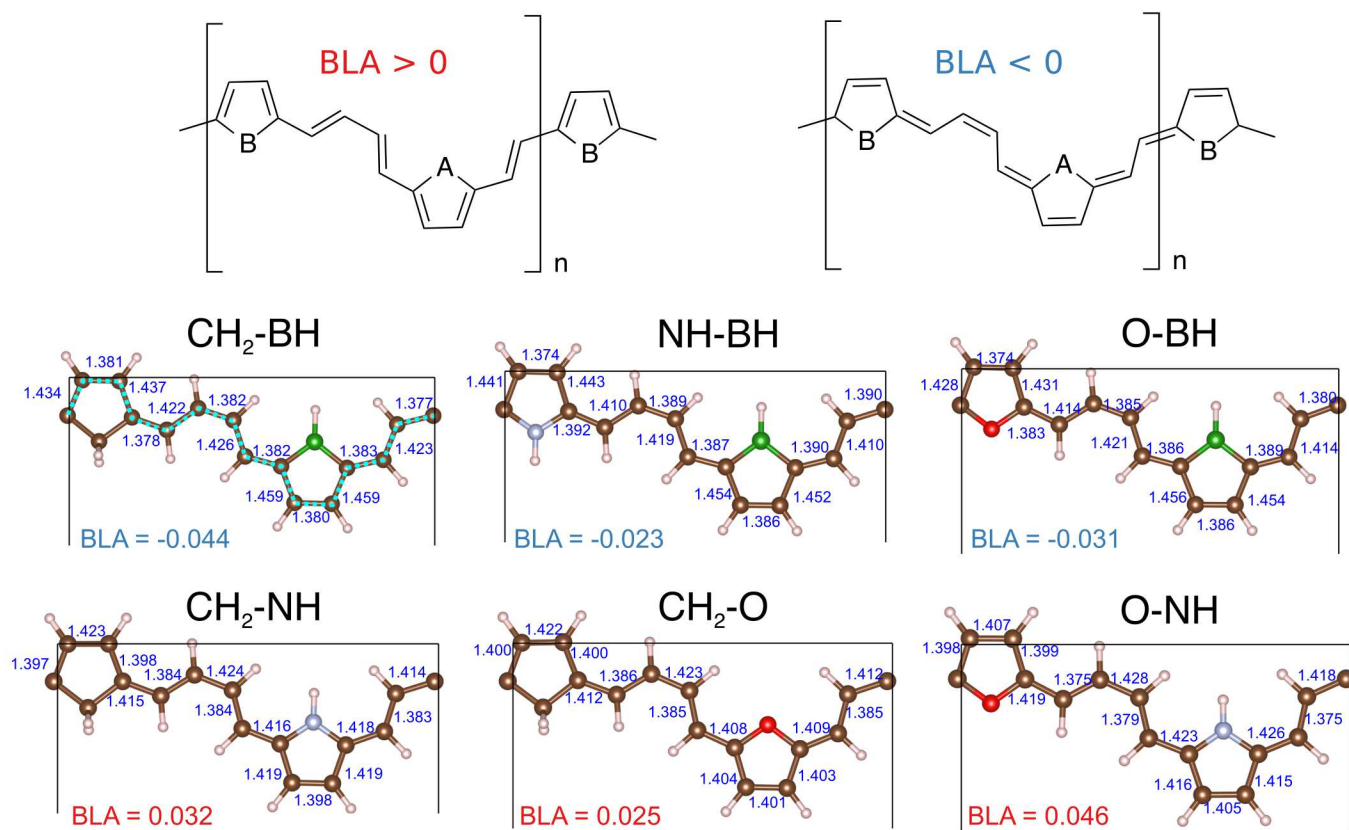


Figure 2: Optimized structures of hybrid heterocyclic polymers with GGA. Bond lengths of C-C bonds (highlighted by broken lines) in Å. The bond length alternation (BLA) is calculated by taking the difference between the bond length of the C-C bond attached to the heterocyclic ring and the C-C bond in the adjacent vinylene linker group. Polymers with boron all have negative values of BLA, showing significant quinoidal character.

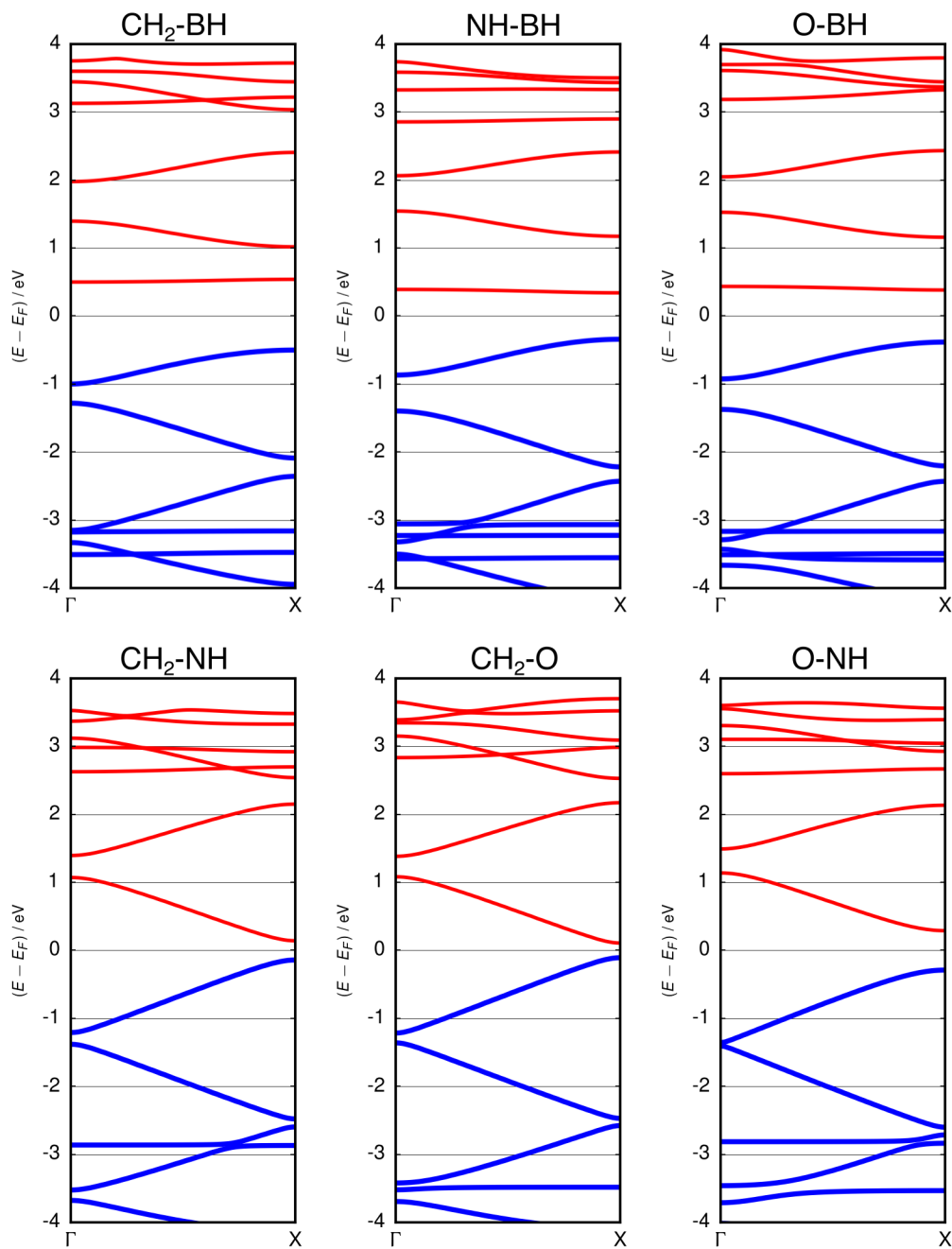


Figure 3: GGA electronic band structures for hybrid heterocyclic polymers ( $r_1 = (\text{CH})_4$ ,  $r_2 = (\text{CH})_2$ ) along the  $\Gamma - X$  path in the irreducible Brillouin zone. The band width of the lowest conduction band for polymers with the BH functional group is significantly smaller than for polymers without boron.

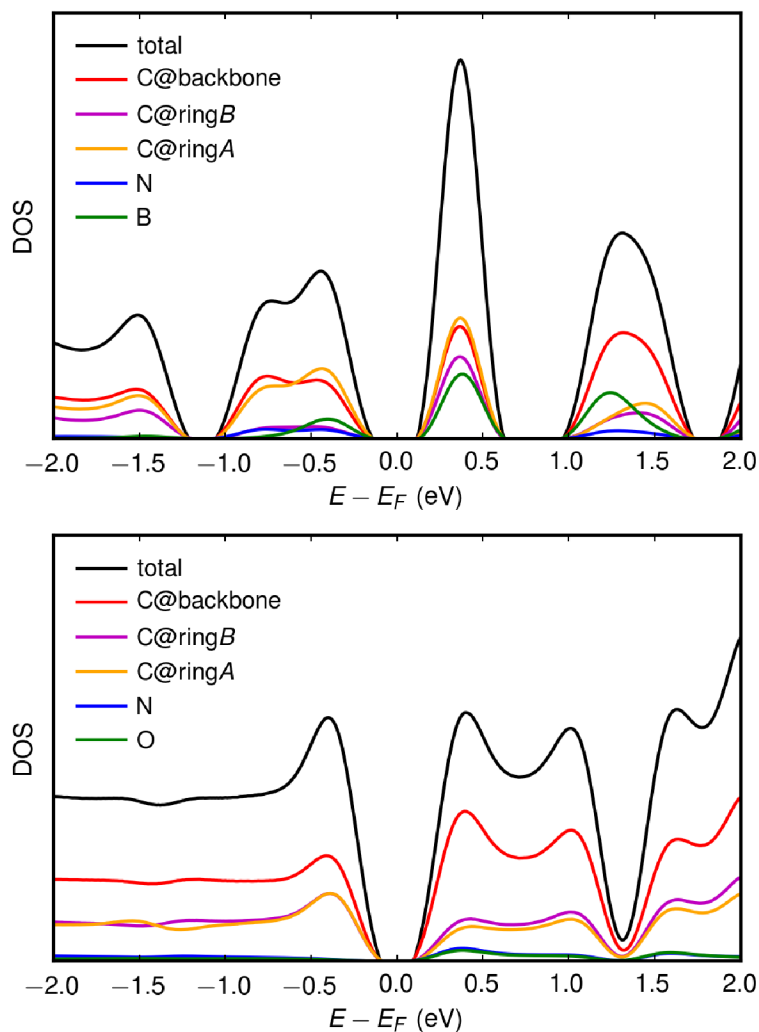


Figure 4: Atom-resolved projected density of states for NH-BH (top) and O-NH (bottom) polymers ( $r1 = (\text{CH})_4$ ,  $r2 = (\text{CH})_2$ ). The boron atom makes substantial contributions to the conduction bands near the Fermi energy.

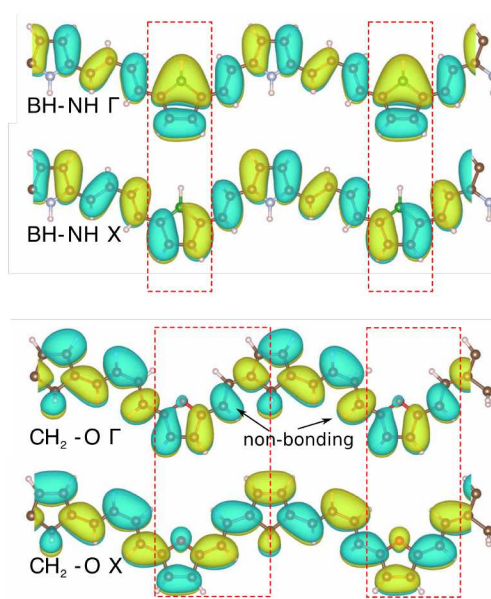


Figure 5: Projected real-space wavefunctions at  $\Gamma$  and X points of lowest conduction band for NH-BH and CH<sub>2</sub>-O polymers. The rectangular boxes outline the regions where the bonding characters of  $\Gamma$  and X are different. The  $\Gamma$  point wavefunction of CH<sub>2</sub>-O polymer shows non-bonding carbon atoms, which results in higher orbital energy.

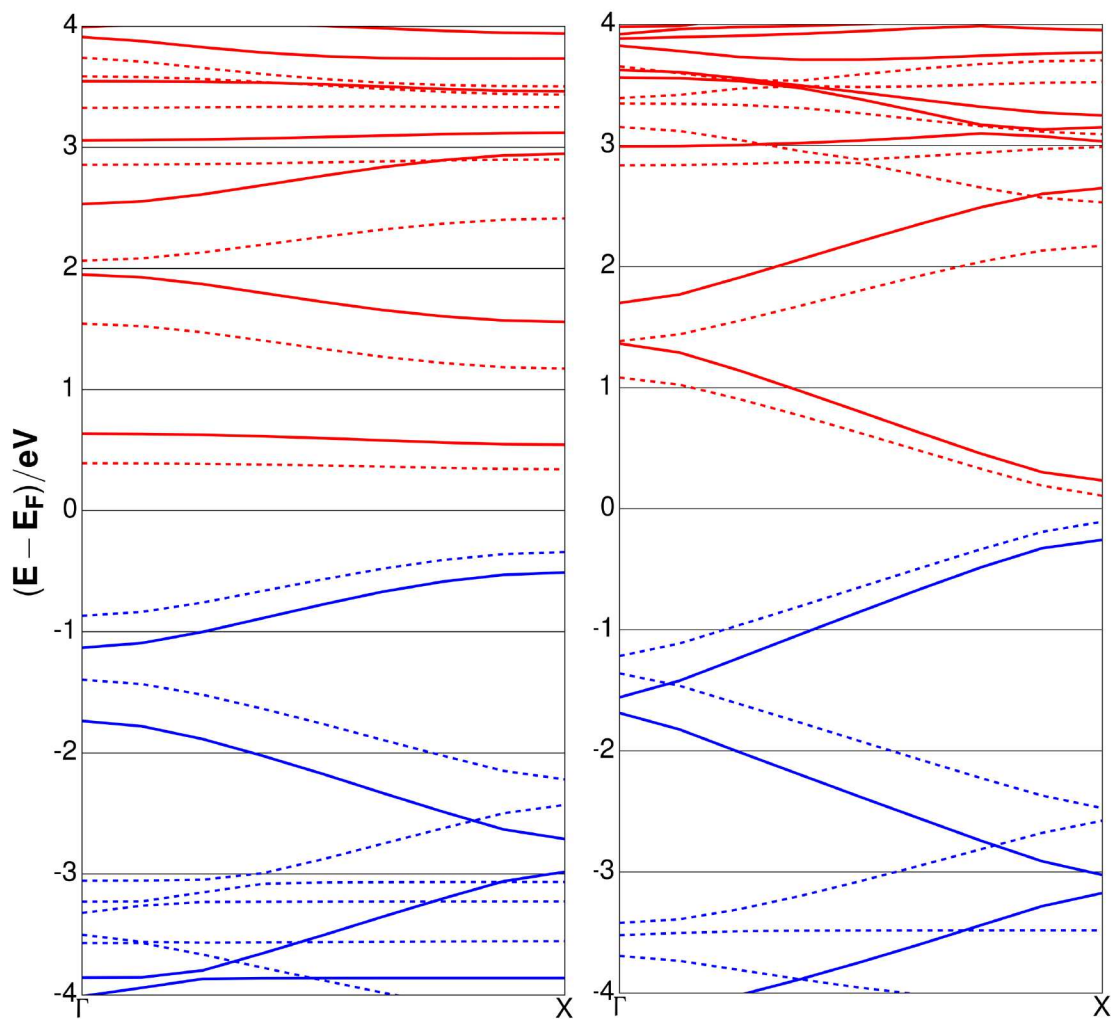


Figure 6: Band structures calculated by HSE (red line) and GGA (black broken line) functionals for a) NH-BH and b) CH<sub>2</sub>-O. The HSE functional tends to cause a rigid shift of the GGA-calculated bands.

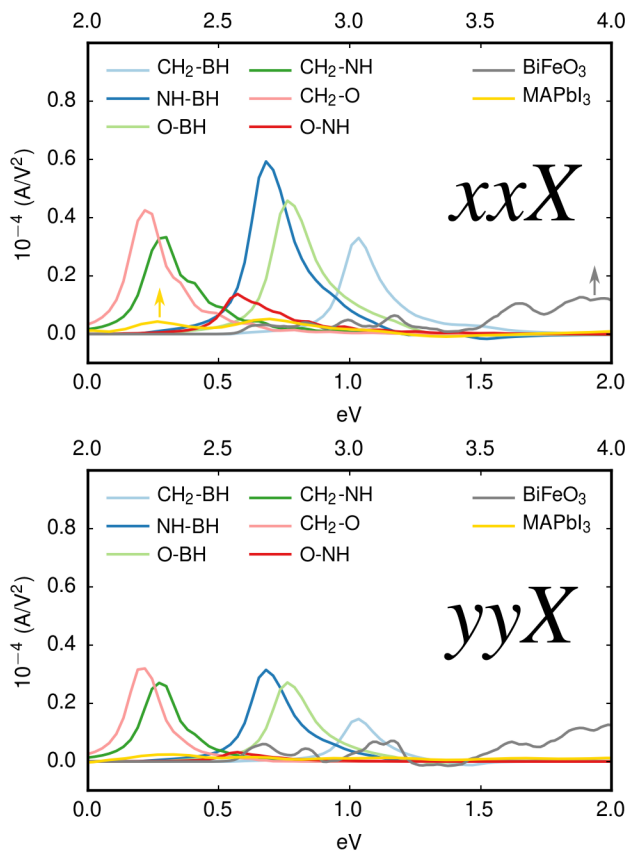


Figure 7: Current density along the polymer chain ( $X$ ) in response to both parallel ( $xxX$ ) and perpendicular ( $yyX$ ) polarized light. The values of current density for benchmark materials,  $\text{BiFeO}_3$  and  $\text{MAPbI}_3$ , are also presented (top  $x$  axis)

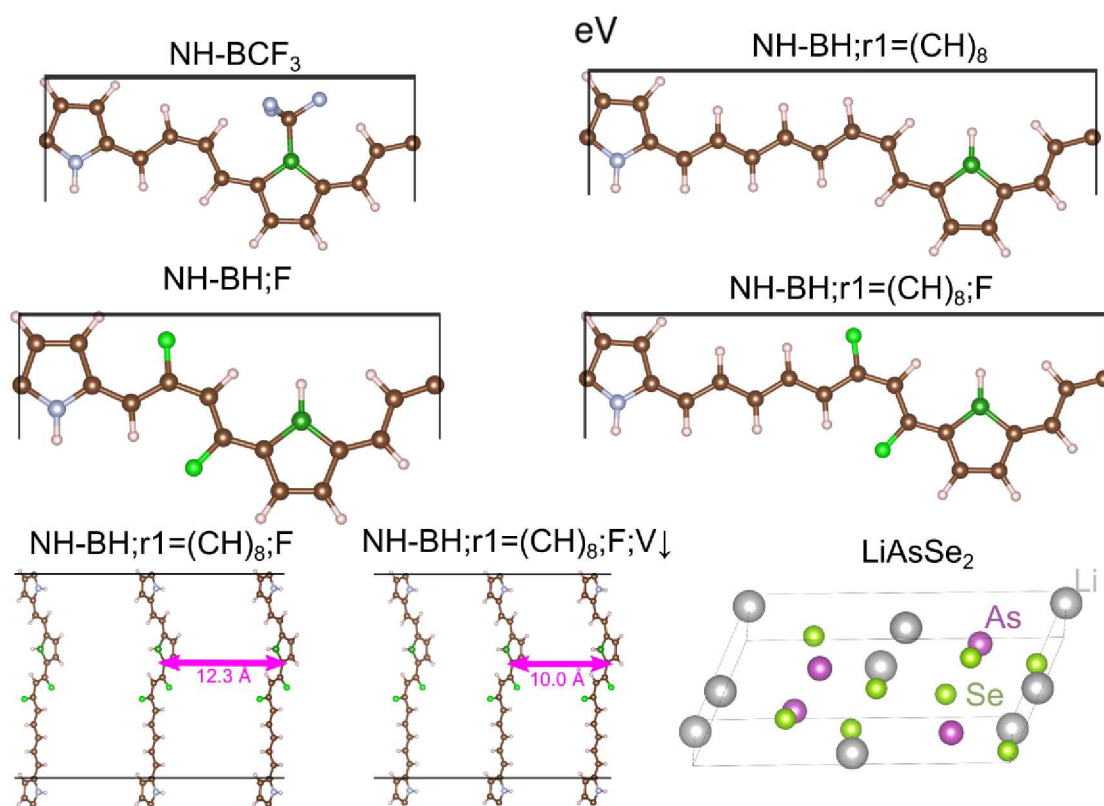
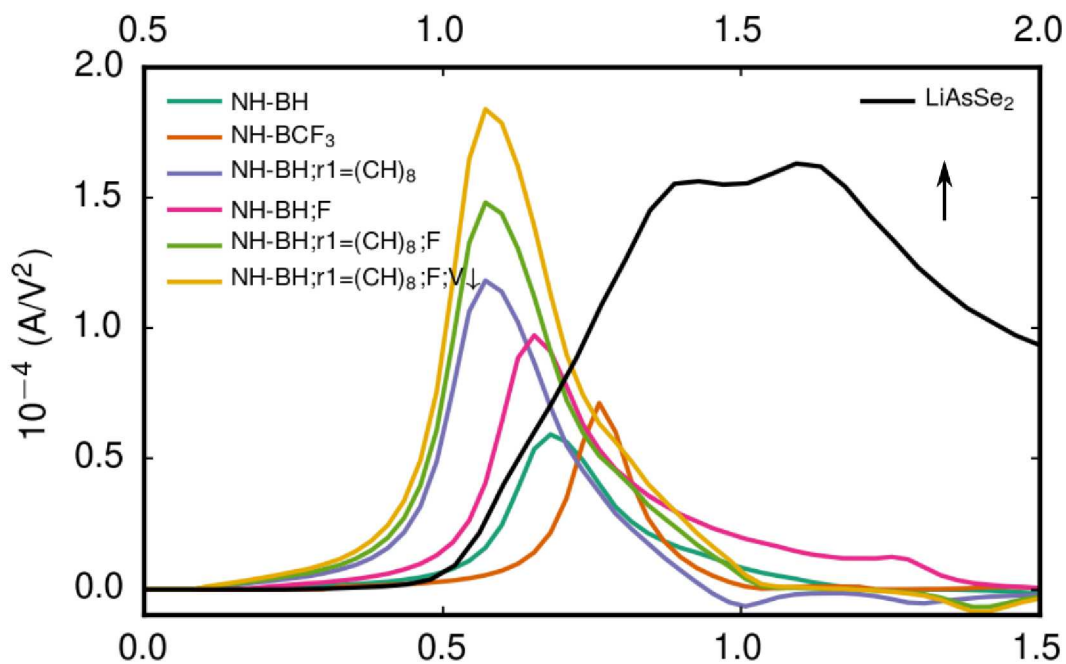


Figure 8: Optimize shift current response through various chemical and physical approaches. Replacing the hydrogen atom attached to the boron with  $-\text{CF}_3$  group gives rise to a larger shift current in  $\text{NH-BCF}_3$  polymer. Polymer with a larger difference between  $r_1$  and  $r_2$  ( $\text{NH-BH};r_1=(\text{CH})_8$ ) also shows stronger response. Replacing some backbone hydrogen atoms with highly electronegative fluorine atoms ( $\text{NH-BH};\text{F}$  and  $\text{NH-BH};r_1=(\text{CH})_8;\text{F}$  polymers) is beneficial. Increasing the polymer density per unit volume by reducing inter-polymer distance ( $\text{NH-BH};r_1=(\text{CH})_8;\text{F};V\downarrow$ ) enhances the response magnitude

